Materials Chemistry and Physics 117 (2009) 228–233

Contents lists available at ScienceDirect

Materials Chemistry and Physics

journal homepage: www.elsevier.com/locate/matchemphys

Effects of severe cold rolling on tensile properties and stress corrosion cracking of 7050 aluminum alloy

D. Wang[a], Z.Y. Ma[a,*], Z.M. Gao[b]

[a] Shenyang National Laboratory for Materials Science, Institute of Metal Research, Chinese Academy of Sciences, 72 Wenhua Road, Shenyang 110016, China
[b] State Key Laboratory of Inorganic Synthesis and Preparative Chemistry, Jilin University, 2699 Qianjin Street, Changchun 130012, China

ARTICLE INFO

Article history:
Received 16 February 2009
Received in revised form 25 April 2009
Accepted 24 May 2009

Keywords:
Aluminum alloys
Cold rolling
Mechanical properties
Stress corrosion cracking

ABSTRACT

7050 aluminum alloy samples were subjected to severe cold rolling (CR) deformation after solution treatment, and then were aged at conventional T6-aging temperature. After CR, shear bands appeared in the matrix and became wide with increasing the CR reduction. The strength of the 7050 samples increased with increasing the CR reduction. The yield and ultimate strengths of the CR sample with a reduction of 67% increased by 16.5% and 9.2%, respectively, compared to those of the T6 sample. Both the residual dislocations and heterogeneously nucleated fine η′ phase particles in the matrix increased the strength of the CR samples. Furthermore, the enlargement in the size and particle interval of the grain boundary precipitates improved the stress corrosion crack (SCC) resistance of the CR samples compared to that of the T6 sample.

1. Introduction

7000 series aluminum alloys have been widely used for aeronautical applications, due to their desirable specific mechanical properties [1]. The mechanical properties of these alloys are determined by the size and distribution of the precipitates via different artificial aging processes. The usual precipitation sequence of the 7000 series Al alloys can be summarized as: Solid solution – GP zone – Metastable η′ – Stable η ($MgZn_2$) [2]. The η′ phase in the peak aged 7000 series Al alloys gave the alloys high strength. However, when alloys were over aged, the precipitates transferred into the η phase and the size of the precipitates increased, decreasing the strength of the alloys [3,4].

Stress corrosion cracking (SCC) of the 7000 series aluminum alloys causes significant service failures in the aerospace industry. Although the SCC mechanism is not completely understood in these alloys, many efforts have been made to correlate the microstructure with the SCC behavior of the alloys. The major microstructural features that affect the SCC resistance are the grain boundary precipitates (GBPs). The SCC resistance could be improved by increasing both the size and interval of the GBPs [5–8].

It is well documented that heat treatments can be used to improve the SCC susceptibility of aluminum alloys in the industrial practice. Over aging, namely T7× temper, is a general method to increase the SCC resistance. However, the T7× temper reduced the strength of the alloys by 10–15% compared to the T6 temper [3]. Several treatment procedures such as the retrogression and re-aging (RRA) [9], step-quench and aging (SQA) treatment [10] and some other thermomechanical treatments (TMTs) were developed to enhance both the strength and the SCC resistance of the 7000 series alloys [11].

Pre-strain prior to the aging is usually applied to the 7000 series alloys in the as-quenched state to relieve quench-induced internal stress [12]. Generally, the value of the pre-strain ranges from 1% to 5%. The dislocations generated in this process could influence the subsequent precipitation process, thereby affecting the mechanical properties of the alloys. In some 7000 series alloys, it was reported that the strain-hardening and the increment in the number of η′ precipitates due to the dislocations generated in the process of the pre-strain led to the strength increase [11,13]. However, the pre-strain also resulted in the generation of equilibrium phase η ($MgZn_2$) on the dislocation network, therefore reducing the amount of solutes for the formation of main hardening phase η′ during subsequent aging, which tended to decrease the mechanical strength of the alloys [14,15]. Furthermore, the over aging treatment on the pre-strained samples would result in the decrease in the strength and SCC resistance of the 7000 series alloy, since some precipitates coarsened in the matrix and the size and particle interval of the GBPs decreased [16].

In despite of a number of reports on the effect of the pre-strain prior to aging, investigation on the effect of severe deformation prior to aging on the mechanical properties and the SCC behavior of the 7000 series alloy is still lacking. In this paper, 7050 aluminum alloy was subjected to severe cold rolling (CR) deformation after

* Corresponding author. Tel.: +86 24 83978908; fax: +86 24 83978908.
E-mail address: zyma@imr.ac.cn (Z.Y. Ma).

0254-0584/$ – see front matter © 2009 Elsevier B.V. All rights reserved.
doi:10.1016/j.matchemphys.2009.05.048

Table 1
Chemical compositions of 7050 Al alloy (wt.%).

Zn	Mg	Cu	Zr	Si	Fe	Al
6.18	2.20	2.21	0. 13	0.11	0.10	Bal.

solution treatment and then aged at the T6 temper temperature, and finally evaluated by tensile tests and the slow strain rate test (SSRT). The aim is to examine the influences of different severe cold rolling reductions prior to aging on the microstructure, tensile properties and SCC resistance of the 7050 aluminum alloy.

2. Experimental

7050 aluminum casting was used as the raw material and the chemical composition of the alloy is shown in Table 1. 20 mm thick plates were cut from the casting and were homogenized at 470 °C for 48 h, and then quenched to room temperature by using water. The homogenized plates were hot-rolled to 6 mm at 430 °C. The hot-rolled samples were solution treated at 470 °C for 1 h in a salt bath furnace and then quenched into water at room temperature. Then the samples were cold rolled in the room temperature to 5, 4, 3, and 2 mm, within 1 h after quenching. After CR, the samples were aged at 120 °C for 24 h immediately. CR2, CR3, CR4, and CR5 referred to the samples cold rolled to the thickness of 2, 3, 4, and 5 mm, respectively. In addition, traditional T6 and T76 treatments were conducted on 6 mm thick hot-rolled plates for the purpose of comparison.

The samples for optical examinations were machined along the cold rolling direction and prepared by mechanical polishing and etching using a solution of 0.5 ml hydrofluoric acid, 15.5 ml nitric acid, 84 ml water, 3 g chromium trioxide. The precipitates in the samples were analyzed by transmission electron microscopy (TEM). Thin foils for TEM were prepared by twin jet-polishing in 30% HNO_3, 70% ethanol solution cooled to −35 °C with liquid nitrogen at 19 V.

Small angle X-ray scattering (SAXS) was carried out on a 18KW Rigaku D/max 2550 PC rotating anode X-ray generator with Cu Kα radiation. The width of the collimation slits are 0.04, 0.03, 0.1 and 0.25 mm. A step scan technique was used with a step width of 0.02°, accounting time of 10 s for each step, the scanning range from 0.08° to 2°. The data were analyzed by NANO-Solver software program.

Dog-bone shaped tensile specimens with a gauge length of 23 mm and a gauge width of 4 mm and a thickness of 2 mm were machined with their axes parallel to the rolling direction. The tensile properties were tested at a strain rate of $1 \times 10^{-3}\ s^{-1}$ by using an SHIMADZU AG-100KNG testing machine.

SCC resistance of the 7050 samples was evaluated using a slow strain rate technique (SSRT) in the air and in a 3.5% NaCl aqueous solution with the gauge length of the specimens being completely immersed during the test. Dog-bone shaped specimens with a gauge length of 10 mm, a width of 3 mm and a thickness of 1 mm were machined from the heat-treated plates with the tensile axes perpendicular to the rolling direction. The SCC resistance tensile tests were conducted at room temperature with a strain rate of $2 \times 10^{-6}\ s^{-1}$ by using an Instron 5848 testing machine. The fracture surfaces of the specimens were observed by scanning electron microscopy (SEM).

3. Results and discussion

Fig. 1 presents optical micrograph of the 7050 alloy samples with various treatments. The grains of the T6 sample were elongated along the hot rolling direction and some recrystallized grains were observed in the matrix (Fig. 1a). For the CR5 sample with a small cold deformation prior to aging, the dislocations formed in the cold rolling process were recovered in the aging process and a lot of sub-grains formed in the original grains (Fig. 1b, the insert shows a magnified view). In the CR4 sample with 33% rolling reduction, some shear bands, aligned at 30–40° to the rolling plane, were observed in the matrix and the grains were elongated along the cold rolling direction (Fig. 1c), which is similar to the results of Hurley and Humphreys [17]. With increasing the cold rolling reduction to 67% (the CR2 sample), the shear bands became remarkably wide and the density of the band increased significantly (Fig. 1d).

Fig. 2 illustrates the tensile properties of the 7050 samples with various heat treatments. Both the yield strength (YS) and ultimate tensile strength (UTS) of the T6 sample were higher than those of the T76 one. Similar result has been reported before [8]. The CR

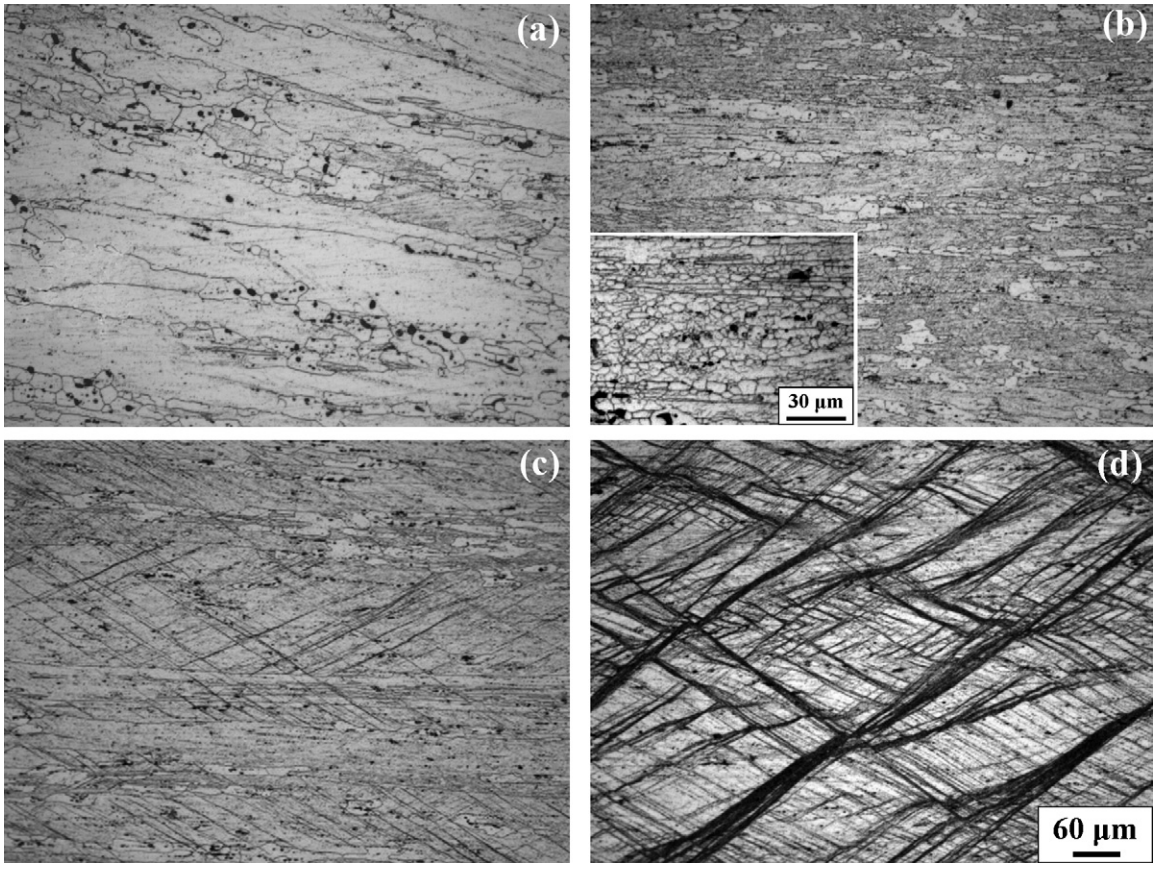

Fig. 1. Optical microstructures of 7050 samples along cold rolling direction at different cold rolling reductions: (a) T6, (b) CR5, (c) CR4, and (d) CR2.

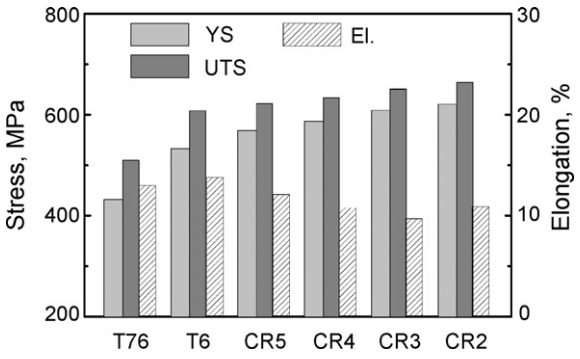

Fig. 2. Tensile properties of 7050 samples with various treatments.

samples with various cold rolling reductions prior to aging exhibited higher YS and UTS compared to the T6 sample. The strength of the CR samples increased as the cold rolling reduction increased. The YS and UTS of the CR2 sample were 621 and 664 MPa, respectively, and increased by 16.5% and 9.2%, respectively, compared to those of the T6 sample. However, the ductility of the CR samples decreased compared to that of the T6 and T76 samples.

Table 2 shows the SSRT results of the samples with various heat treatments in the air and 3.5% NaCl solution at a strain rate of $2 \times 10^{-6}\ s^{-1}$. The UTS values of the samples tested in the air were lower than those in Fig. 2 because these samples were tested perpendicular to the rolling direction at a lower strain rate. The UTS values of the samples tested in the 3.5% NaCl solution were slightly lower than those tested in air, similar to the other reports [6,11]. However, the elongations in the 3.5% NaCl solution were remarkably lower than those in the air. The elongation of the T76 sample

Table 2
Transverse mechanical properties of differently treated 7050 Al alloy at a strain rate of $2 \times 10^{-6}\ s^{-1}$.

Pre-strain (%)	UTS (MPa)		Elongation (%)		
	In air	In 3.5% NaCl	In air	In 3.5% NaCl	$r_{sol/air}$ (%)
T76	489	484	9.1	8.6	94.3
T6	588	591	8.6	5.8	67.4
CR4	624	614	6.6	4.6	69.7
CR2	636	624	4.4	3.4	77.3

in the 3.5% NaCl solution was the largest among these samples. The CR samples exhibited smaller elongation than the T76 and T6 samples. Moreover, the elongation of the CR samples decreased with the cold rolling reduction increased.

Previously, some researcher used the elongation to evaluate the SCC resistance [18]. Larger elongation of the sample tested in the 3.5% NaCl solution means that the sample has better SCC resistance. Although the elongation of the CR samples was lower than that of the T6 sample in the 3.5% NaCl solution, the CR samples also exhibited lower elongation than the T6 sample in the air. This indicated that the elongation in the 3.5% NaCl solution is not a proper parameter to evaluate the SCC resistance for this study. Similar observations have been reported in our previous study [11].

Similar to our previous study [11], we used an index $r_{sol/air}$ to evaluate the SCC resistance, which is the ratio of the elongations of the samples tested in the 3.5% NaCl solution and in air. The greater the $r_{sol/air}$ value is, the better the SCC resistance is, as shown in Table 2. The $r_{sol/air}$ value of 1 implies that the material exhibits no SCC susceptibility. The T76 sample had the highest $r_{sol/air}$ value, indicating that the T76 sample had the best SCC resistance. The $r_{sol/air}$ value of the T6 sample was only 67.4% and much lower than of the

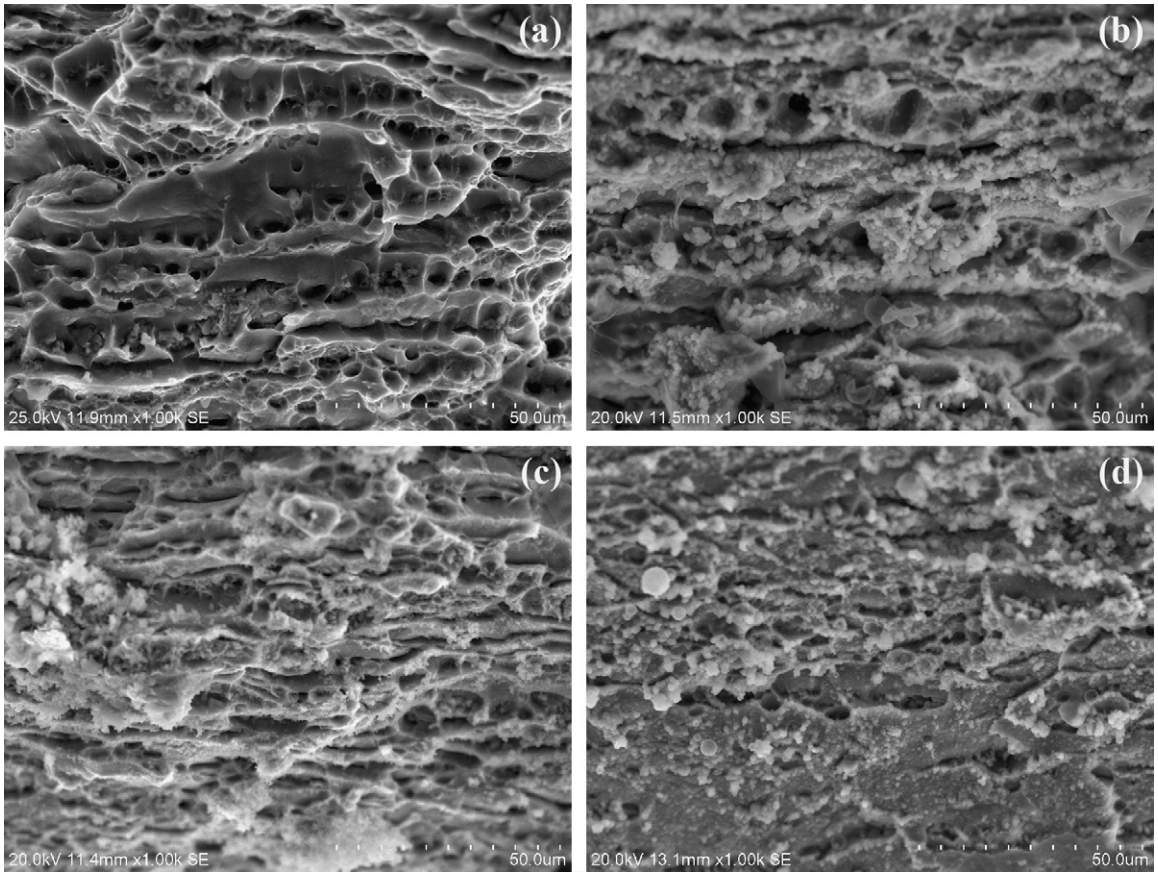

Fig. 3. SEM micrographs showing SSRT fracture surfaces of 7050 samples with various treatments in 3.5% NaCl solution: (a) T76, (b) T6, (c) CR4, and (d) CR2.

T76 sample, indicating that the SCC resistance of the T6 sample was worse than that of the T76 sample. Similar results have been reported in the previous studies [7,8]. For the CR samples, although the elongations were lower than that of the T6 sample (Table 2), the $r_{sol/air}$ values were larger than that of the T6 sample, indicative of improved SCC resistance. With increasing the cold rolling reduction, the $r_{sol/air}$ values increased, though the elongation of the samples decreased. The $r_{sol/air}$ value of the CR2 sample was 77.3% and increased by about 10% compared to the T6 sample.

Fig. 3 presents the typical tensile fracture surfaces of the T76, T6 and CR samples tested in the 3.5% NaCl solution. The fracture surface of the T76 sample was dominated by intergranular microvoid coalescences (Fig. 3a). This is attributed to the preferential deformation of the precipitate free zones around the grain boundary area [6]. Furthermore, some large dimples and cleavage facets were also observed on the fracture surface of this sample. In contrast, the fracture surface of the T6 sample was dominated by the intergranular fracture with severe corrosion, showing the typical brittle fracture and SCC attack (Fig. 3b). For the CR4 sample, some intergranular cracks were present in the fracture surface and there were also some microvoids on the grain boundaries, furthermore, some dimples were also observed. However, for the CR2 sample, the fracture surface was different from that for the other samples. Some intergranular microvoid coalescences were observed on the grain boundaries. But these microvoids were smaller than those in the T76 sample. The fracture surface was dominated by the cleavage, indicating that the sample had the brittle fracture character.

Fig. 4 shows the TEM images within the grains of the T6, T76 and CR samples. For the peak aged (T6) 7050 alloy, the η′ phase was the main precipitate and some GP zones remained in the matrix, the precipitates were homogeneously distributed (Fig. 4a). For the T76 sample with an over aging the average size of the precipitates increased. Some large precipitates were homogeneously distributed within the grains (Fig. 4b). The strength of the T76 sample decreased because the size of the precipitates increased compared to the T6 sample. Similar result has been previously reported [19].

For the CR4 sample with a 33% cold rolling reduction prior to the aging, many dislocations were generated in the cold rolling process and remained in the matrix after the aging (Fig. 4c). Some large precipitates were heterogeneously distributed in the dislocation network. The residual dislocations in the matrix would be one of the reasons leading to the increase in the strength of the sample (Fig. 2). For the CR2 sample having a 67% cold rolling reduction, there were more residual dislocations in the matrix and the strength of the samples increased (Fig. 2). In addition, the number of large precipitates in the dislocation network increased (Fig. 4d).

Fig. 5 shows the average density distribution of the particles in various samples measured by small angle X-rays scattering. The particle distribution was very different in these samples. For the T6 sample, the precipitates were very small. The average diameter of the particles was 4.1 nm, and the particle distribution was also very homogeneous. This result is consistent with the TEM observation (Fig. 4a). For the T76 sample, the precipitates were the largest among these samples with the average diameter of the particles being 13.8 nm. Different from that in the T6 sample, the size distribution of the precipitates in the T76 sample is within a wide range. However, for the CR samples with the same aging process of the T6 sample, the distribution of the precipitates was quite different from that of the T6 sample. The diameter of the precipitates

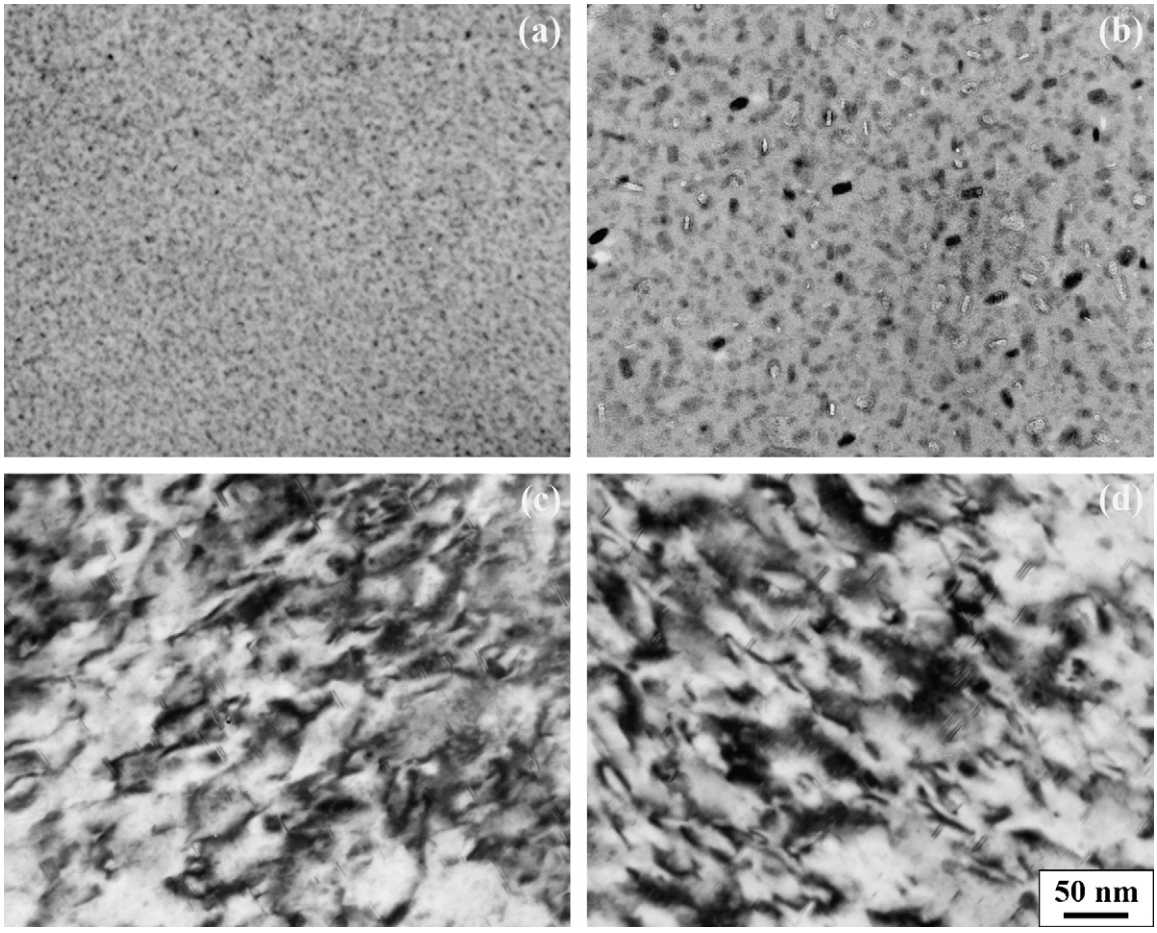

Fig. 4. TEM micrographs showing precipitates within grains of 7050 samples with various treatments: (a) T6, (b) T76, (c) CR4, and (d) CR2.

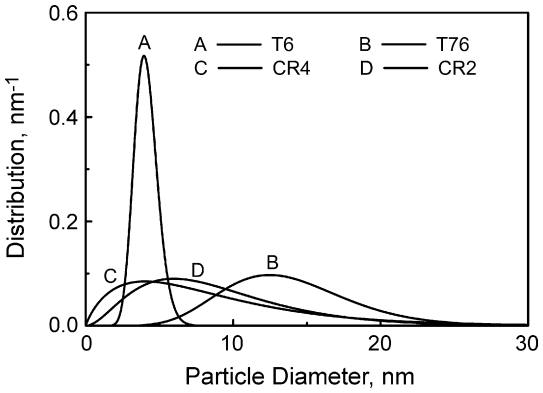

Fig. 5. Precipitate distribution of 7050 samples with various treatments measured by small angle X-rays scattering.

was distributed in a wider region than that for the T76 sample. The average diameter of the precipitates in the CR4 sample was 8.6 nm, larger than that in the T6 sample. Some larger particles had the similar sizes to those in the T76 sample, which were also observed by TEM (Fig. 4c). Furthermore, some finer particles with the size being smaller than that in the T6 sample were also revealed in the CR4 sample. Similar phenomenon was observed in the CR2 sample. The average diameter of the precipitates in the CR2 sample was determined to be 9 nm and increased slightly compared to that in the CR4 sample, with the content of the larger particles increasing. This is consistent with the TEM observations (Fig. 4c and d).

It is well documented that the strengthening precipitates in the T6 temper 7000 series alloys are GP zone and η' phase [2]. For the CR samples, many dislocations were generated in the cold rolling process. The dislocations would remain in the matrix after the aging treatment because the aging temperature was not high enough to recover all the dislocations. The residual dislocations in the samples would increase the strength of the samples and decrease the elongation. Furthermore, although the quenching vacancies are easily annihilated in the dislocations [15], the dislocations are of benefit to the heterogeneous nucleation of the precipitates. Therefore, more number of fine η' phase could nucleate and grow in the CR samples than the T6 sample, even though the aging process was the same (Fig. 5). The increment of the fine precipitates in the CR samples was another reason for the strength increase of the sample. In addition, some large precipitates were also presented in the dislocation network (Fig. 4c and d), due to the heterogeneous nucleation and the fast diffusion of the solutes in the dislocations. The CR2 sample had the highest dislocation density in the matrix due to the largest cold rolling reduction. Furthermore, the number of large precipitates increased in the matrix. Although the large precipitates could decrease the strength of the samples, the residual dislocation and the increment of the fine η' phase led to the increase in the strength of the CR samples.

Fig. 6 illustrated the GBPs in the 7050 samples with various heat treatments. The precipitates on the grain boundaries of the T6 sample were small and continuously distributed (Fig. 6a). However, in the T76 sample the grain boundaries were decorated with the coarse and discontinuously distributed particles (Fig. 6b), which is similar to the previous reports [5,7]. The GBPs in the CR4 sample (Fig. 6c) were larger than those in the T6 sample (Fig. 6a) and the particle interval was also larger than that in the T6 sample. With increasing the cold rolling reduction, the size of the GBPs increased slightly and the particle interval also increased (Fig. 6d). All of the GBPs in the CR samples were smaller than those of the T76 sample.

Similar to the precipitates within the grains, the GBPs were also influenced by the dislocations. Besides the dislocations presented within grains, a great amount of dislocations also aggregated around the grain boundaries. The dislocations around the grain boundaries also provided heterogeneous nucleation sites for the GBPs which would grow in the aging process and finally form discontinuously distributed GBPs. Furthermore, the dislocations were also of benefit to the solute element diffusion to the grain boundaries. The high density of dislocations not only was beneficial to the growth of the GBPs, but also decreased the width of the precipitate free zone (PFZ) via the solute transfer from the grain interiors to the grain boundaries (Fig. 6c and d). That is similar to our previous work [11,16].

For the 7000 series aluminum alloys, the SCC resistance was related to the GBPs. The mechanism of the SCC in the Al–Zn–Mg–Cu alloys was thought to be both anodic dissolution and hydrogen embrittlement [20]. The precipitates on the grain boundaries are Mg-rich phases in these alloys, which have the electrode potential different from the Al matrix [7,21]. This would result in the anodic dissolution and form critical defects in the first stage of the SCC process in the aqueous chloride solutions. Furthermore, the hydrogen produced in the crack tip also leads to the hydrogen embrittlement on the grain boundaries.

Song et al. [21,22] reported that the element Mg on the grain boundaries had larger electronegativity differences between Mg and H atom than that between Al and H atom. Therefore, Mg on the grain boundaries could increase the amount of hydrogen absorbed and consequently accelerate its diffusion and enhance the solution degree of hydrogen on the grain boundaries. This may result in the embrittlement of the grain boundaries and accelerate the growth of the stress corrosion cracks. However, the increase in the size and interparticle spacing of the GBPs could decrease the anodic dissolution speed, and acted as the trapping sites for atomic hydrogen and created molecular hydrogen bubbles, which would reduce the concentration of the atomic hydrogen on the grain boundaries. T76 sample had the largest GBPs and interparticle spacing among these samples. Therefore, the SCC resistance of the T76 sample was the best. For the CR samples, especially the CR2 sample, both the size and interval of the GBPs increased compared to the T6 sample. Therefore, the SCC resistance of the CR samples was better than that of the T6 sample.

Furthermore, differently from the T6 and T76 sample, the CR samples had many dislocations in the matrix (Fig. 4c and d). The dislocations were not only present within the grains, but also aggregated around the grain boundaries, which formed the network in the matrix. However, the role of dislocations in the SCC resistance was seldom investigated. Talianker and Cina [23] found that the SCC resistance of 7000 series alloy increased via the RRA heat treatment from the T651 temper alloy. Most of the dislocations in the T651 temper alloys were annihilated in the RRA process. Therefore, they deduced that the dislocations adjacent to the grain boundaries decreased the SCC resistance of 7000 series alloys. However, they did not report the variations of the GBPs in those alloys, which had a benefit for the SCC resistance based on most of the recent investigations [7,8]. Albrecht et al. suggested that the mobile dislocations generated in the tip of the crack would improve the hydrogen diffusion in the matrix [24]. For the CR samples, the dislocation network was present in the matrix before SSRT. The hydrogen diffused along the grain boundaries possibly diffused into the grains along the dislocation network. The mobile dislocations generated in the tip of the crack would also interact with the original dislocation network to make the hydrogen diffuse into the grains. Within the grains, many Mg-rich η' phase particles were present in the dislocation network due to the heterogeneous nucleation at the dislocations. They would also easily absorb the hydrogen like the Mg-rich phase on the grain boundaries. In this case, it is likely that the hydrogen diffusion along the grain boundaries was further inhibited in the SSRT. For the CR samples, the SCC resistance was increased compared to the T6 sample. The increment of size and interparticle spacing of the GBPs was of benefit to their SCC resistance as discussed above.

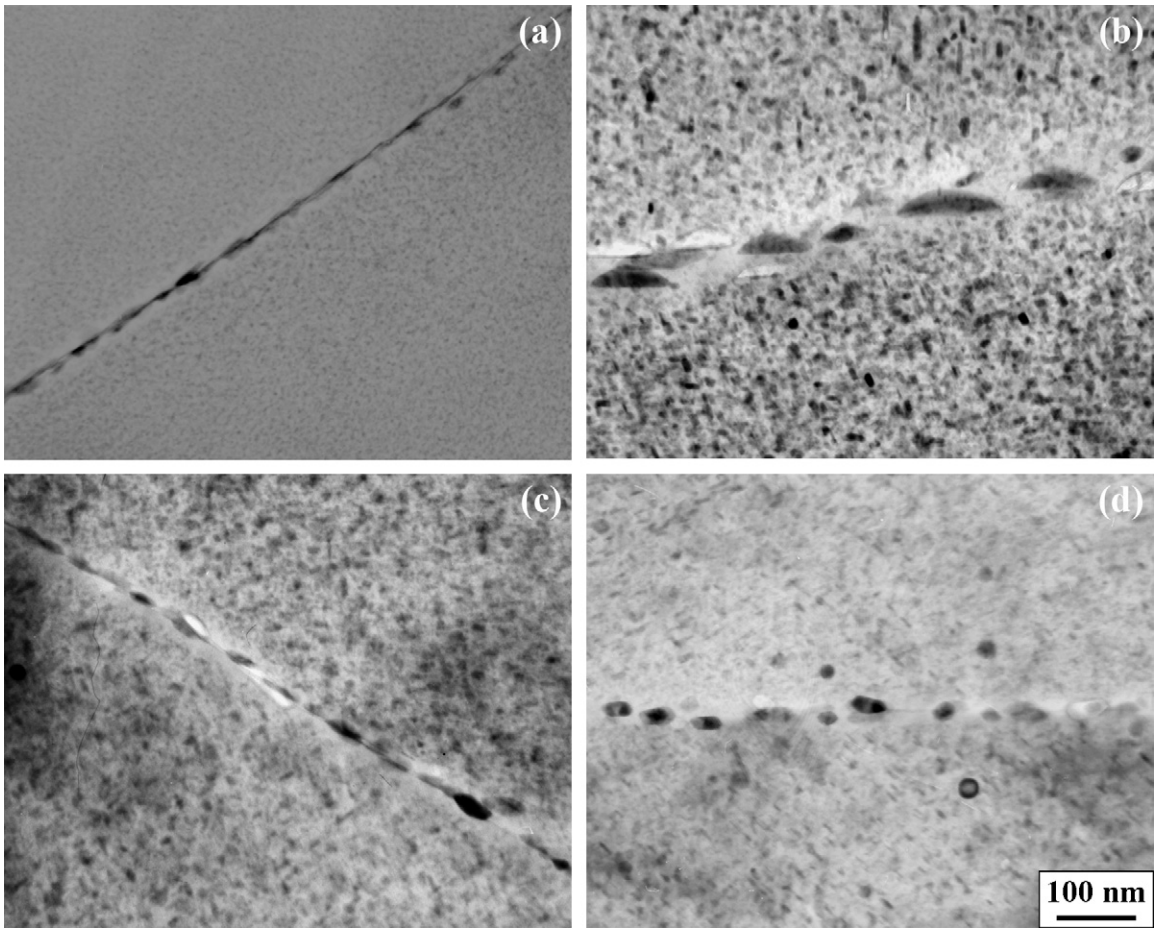

Fig. 6. TEM micrographs showing grain boundary precipitates of 7050 samples with various treatments: (a) T6, (b) T76, (c) CR4, and (d) CR2.

However, the effect of the dislocations on the SCC resistance is not well understood and needs more detailed experimental investigation.

4. Conclusions

1. Shear bands appeared in the matrix when 7050 alloy was cold rolled to a reduction of 33% prior to the aging. When the cold rolling reduction increased to 67%, the shear bands in the matrix became significantly wide and were distributed in the whole sample.
2. The strength of the CR samples with cold rolling prior to aging increased with increasing the cold rolling reduction. The YS and UTS of the CR2 sample increased by 16.5% and 9.2%, respectively, compared to those of the T6 sample.
3. The size distribution of the precipitates in the CR samples was in a wider range than that of the T76 sample. The residual dislocations and the increment of fine precipitates in the matrix contributed the strength increase of the CR samples.
4. The enlargement in the size and particle interval of the grain boundary precipitates improved the SCC resistance of the CR samples compared to the T6 sample.

Acknowledgment

The authors gratefully acknowledge the support of National Basic Research Program of China under grant no. 2005CB623708.

References

[1] J.E. Hatch (Ed.), Aluminum Properties and Physical Metallurgy, American Society for Metals, Ohio, 1984.
[2] G. Sha, A. Cerezo, Acta Mater. 52 (2004) 4503.
[3] M. Dixit, R.S. Mishra, K.K. Sankaran, Mater. Sci. Eng. A 478 (2008) 163.
[4] J. Grobner, L.L. Rokhlin, T.V. Dobatkina, R. Schmid-Fetzer, J. Alloys Compd. 443 (2007) 108.
[5] M. Puiggali, A. Zielinski, J.M. Olive, E. Renauld, D. Desjardins, M. Cid, Corros. Sci. 40 (1998) 805.
[6] M. Bobby Kannan, V.S. Raja, J. Mater. Sci. 41 (2006) 5495.
[7] B.L. Ou, J.G. Yang, M.Y. Wei, Metall. Mater. Trans. 38A (2007) 1760.
[8] J.C. Lin, H.L. Liao, W.D. Jehng, C.H. Chang, S.L. Lee, Corros. Sci. 48 (2006) 3139.
[9] B.M. Cina, U.S. Patent No. 3,856,584 (1974).
[10] B.L. Ou, J.G. Yang, C.K. Yang, Mater. Trans. 41 (2000) 783.
[11] D. Wang, D.R. Ni, Z.Y. Ma, Mater. Sci. Eng. A 494 (2008) 360.
[12] A. Deschamps, Y. Brechet, P. Guyot, F. Livet, Z. Metallkd. 88 (1997) 601.
[13] S. Kassim, A. Rubaie, E.K.L. Barroso, L.B. Godefroid, Int. J. Fatigue 28 (2006) 934.
[14] G. Waterloo, V. Hansen, J. Gjonnes, S.R. Skjervold, Mater. Sci. Eng. A303 (2001) 226.
[15] A. Deschamps, F. Livet, Y. Brechet, Acta Mater. 47 (1999) 281.
[16] D. Wang, Z.Y. Ma, J. Alloys Compd. 469 (2009) 445.
[17] P.J. Hurley, F.J. Humphreys, Acta Mater. 51 (2003) 1087.
[18] T.C. Tsai, T.H. Chuang, Mater. Sci. Eng. A225 (1997) 135.
[19] M.J. Starink, S.C. Wang, Metall. Acta Mater. 51 (2003) 5131.
[20] D. Najjar, T. Magnin, T.J. Warner, Mater. Sci. Eng. A 238 (1997) 293.
[21] R.G. Song, W. Dietzel, B.J. Zhang, W.J. Liu, M.K. Tseng, A. Atrens, Acta Mater. 52 (2004) 4727.
[22] R.G. Song, M.K. Tseng, B.J. Zhang, J. Liu, Z.H. Jin, K.S. Shin, Acta Mater. 44 (1996) 3241.
[23] M. Talianker, B. Cina, Metall. Trans. 20A (1989) 2087.
[24] J. Albrecht, I.M. Bernstein, A.W. Thompson, Metall. Trans. 13A (1982) 811.